

# Toward A Scalable Exploratory Framework for Complex High-Dimensional Phenomics Data

Methun Kamruzzaman\*, Ananth Kalyanaraman†, Bala Krishnamoorthy‡ and Patrick Schnable§

## Abstract

Phenomics is an emerging branch of modern biology, which uses high throughput phenotyping tools to capture multiple environment and phenotypic trait measurements, at a massive scale. The resulting high dimensional data sets represent a treasure trove of information for providing an indepth understanding of how multiple factors interact and contribute to control the growth and behavior of different plant crop genotypes. However, computational tools that can parse through such high dimensional data sets and aid in extracting plausible hypothesis are currently lacking. In this paper, we present a new algorithmic approach to effectively decode and characterize the role of environment on phenotypic traits, from complex phenomic data. To the best of our knowledge, this effort represents the first application of topological data analysis on phenomics data.

We applied this novel algorithmic approach on a real-world maize data set. Our results demonstrate the ability of our approach to delineate emergent behavior among subpopulations, as dictated by one or more environmental factors; notably, our approach shows how the environment plays a key role in determining the phenotypic behavior of one of the two genotypes.

Source code for our implementation and test data are freely available with detailed instructions at <https://xperthut.github.io/HYPPO-X>.

## 1 Introduction

High-throughput technologies are beginning to change the way we observe and measure the natural world in life sciences. In medicine, physicians are using imaging and other specialized sampling devices to keep a longitudinal log of patients' drug/therapy response and other disease-related *phenotypes*. In agricultural biotechnology, phenotyping technologies such as cameras and LiDARs are being used to measure physiological and morphological features of a crop on the field. Further, advancements in *genotyping* technologies (sequencing) have made it possible to characterize and track genetic diversity and changes at a high resolution, and decode genetic markers key to performance traits. Taken together, advancements in these technologies are leading to a rapid explosion of high-dimensional data, obtained from a variety of sources.

A distinctive feature of these inherently high-dimensional data sets is that their generation is motivated more based on the availability and easy access to high-throughput technology (as opposed to specific working hypotheses). While there are some broad high-level questions or research themes that motivate the collection of data, the specific questions that relate to testable hypothesis and eventual discoveries (e.g., what genetic variations impact a physical trait, or how a combination of environmental variables control a phenotype) are *not* readily available *a priori*.

---

\*School of Electrical Engineering & Computer Science, Pullman, WA, 99164, USA

†School of Electrical Engineering & Computer Science, Pullman, WA, 99164, USA

‡Department of Mathematics and Statistics, Vancouver, WA, 98686, USA

§Department of Agronomy, Department of Genetics, and Department of Development and Cell Biology, Ames, IA, 50011, USA

Individuals	Genotype (/SNPs)	Phenotypic trait values observed at different timestamps and environmental conditions
Crop 1		
Crop 2		
...		
Crop n		

Figure 1: Schematic table view of a multi-dimensional phenomics data set.

Consider the case of plant phenomics [7, 17]. Understanding how different crop *genotypes* ( $G$ ) interact with *environments* ( $E$ ) to produce varying different performance traits (*phenotypes* ( $P$ )) is a fundamental goal of modern biology ( $G \times E \rightarrow P$ ) [4, 21]. To address this fundamental albeit broad goal, plant biologists and farmers have started to widely deploy an array of high-throughput sensing technologies that measure tens of crop phenotypic traits on the field (e.g., crop height, growth characteristics, photosynthetic activity). These technologies, comprising mostly of camera and other recording devices, generate a wealth of images (visual, infrared, thermal) and time-lapse videos, that represent a detailed set of observations of a crop population as it develops over the course of the growing season. Additionally, environmental sensors help in collecting daily field conditions that represent the growth conditions. Furthermore, through the use of sophisticated genotyping technologies, the genotypes of the different crop varieties are also cataloged. Fig. 1 shows a table view of a typical phenomics data set.

From this medley of plant genotypes, phenotypes, and environmental measurements, scientists aim to extract plausible hypotheses that can be field-tested and validated. However, the task remains significantly challenging, due to the dearth of automated software capabilities that are capable of handling complex, high-dimensional data sets. Scatter plots and correlation studies can reveal only high-level correlations and behavioral patterns/differences within data. However, it is common knowledge that different individuals or subgroups of individuals behave differently under similar stimuli. For instance, while it is useful to know that a given environmental variable (e.g., humidity) shows an overall positive correlation to a performance trait (phenotype), such high-level correlations obfuscate the variations within a population—e.g., how different subgroups or genotypes respond to different environmental intervals; or how one environmental variable interacts/interplays with another to affect the performance trait; or how the same genotype expresses variability in their performance in different environments. In fact, the need to identify such intra-population variations is what drives the generation of high-dimensional data in the area of phenomics [7, 17, 24].

## 1.1 Contributions

In this paper, we present a novel computational approach for extracting hypotheses from high-dimensional data sets such as phenomics collections. We formulate the problem of hypothesis extraction as one of: (a) identifying the key connected structural features of the given data, and (b) exploring the structural features in a way to facilitate extraction of plausible hypotheses.

**Structure Identification:** Our approach uses emerging principles from *algebraic topology* as the basis to observe and discern structural features from high-dimensional data. Algebraic topology is the field of mathematics dealing with the shape and connectivity of spaces [22, 9]. There are multiple important properties of topology that make it particularly effective for extracting structural features from large, high-dimensional data sets (see Section 5).

**Topological Object Exploration:** While topological representations offer a compact way to represent and explore the data, the process of navigation and hypothesis extraction is an un-

explored problem—one that is nontrivial with no current solutions. In this paper, we formulate this problem formally as one of identifying *maximal interesting paths* in a topological object. This novel formulation and a related algorithm allows our approach to systematically identify and evaluate potentially interesting features in topological representations.

**Experimental Results:** To demonstrate its effectiveness, we conducted a thorough experimental evaluation of our topological exploratory approach on a real-world maize data set, which contains environmental and phenotypic observations for two genotypes in two geographic locations (Kansas (KS) and Nebraska (NE)), over a period of 100 days—for a total of 400 “points”. Our automated approach generates the topological object that clearly separates the genotypes of both locations. In fact, the interesting paths of the topological object identified by our method demonstrates the ability to: (i) identify the developmental and environmental stages of separation between the two genotypes, and between the two locations; and (ii) identify subtle variations in the behavior of individuals (or groups) within the subpopulations defined by genotypes and locations. Note that these findings are achieved in an entirely *unsupervised* manner by our approach.

We have implemented our approach as a software tool, which we call *Hyppo-X*<sup>1</sup>. The tool is available as open source on the following website: <https://xperthut.github.io/HYPP0-X>.

Even though we demonstrate the utility of our approach in the context of plant phenomics, our approach can be applied more broadly to other similar application contexts where the goal is to derive plausible hypotheses from complex, high-dimensional biological data sets.

The rest of the paper is organized as follows: Section 2 presents our algorithms and implementation details of our topological exploratory framework. Section 3 presents the model to extract the hypothesis from the topological object constructed in Section 2 in the form of interesting paths. Section 4 presents a thorough experimental study and evaluation of our framework on a real-world maize data set. Section 5 reviews related tools used in phenomics research.

## 2 Building Compact Topological Representations

The first step in our approach is to construct topological representations using the connectivity properties of the data. The motivation is to obtain higher order structural information about the high-dimensional data prior to gleaning hypotheses. We adopt and adapt the Mapper algorithmic framework [25] for this purpose, and output our representations in the form of *simplicial complexes* (defined below). In what follows, we describe the details of our implementations of the individual steps of the framework. Fig. 2 is a schematic illustration of our approach.

**Input:** We are given a set of  $n$  points  $\mathcal{S}$  in a  $d$ -dimensional space, representing the space of interest  $X$ . In the case of phenomics, a *point*  $x \in \mathcal{S}$  represents a crop individual that is measured at a particular time  $t$ , and the dimensions represent the attributes which describe the point at that time. These include a set  $E$  of  $m$  factors (e.g., time, temperature, humidity, etc.), and a performance trait, the phenotype  $p$  (e.g., plant height or growth rate). Note that these dimensions represent continuous variables<sup>2</sup>.

**Output:** We aim to create a highly compact coordinate-free representation of  $X$  as a *simplicial complex*, using a clustering (overlapping) of the points in  $X$  (represented by  $P$  here).

A *simplicial complex* is a collection of simplices (nodes, edges, triangles, tetrahedra, etc.) that fit together nicely—all subsimplices of each simplex are included in the collection, and any two simplices that intersect do so in a lower dimensional subsimplex. Specifically, each cluster is represented by a node (0-simplex). Whenever two clusters have a non-empty intersection, we add an edge (1-simplex), and when three clusters intersect, we add a triangle (2-simplex), and so on.

We now provide the main algorithmic details of the approach.

---

<sup>1</sup>Stands for “Hypothesis Extraction”.

<sup>2</sup> A point may also have other non-continuous or static variables (e.g., the genotype). For the purpose of our topological representations we will use only the continuous variables.

## 2.1 Filtering

The first component of the framework is a continuous function  $f : X \rightarrow Z$  to a real-valued parameter space  $Z$ , called the *filter function*. For each factor  $Z_j$ , we define a filter function  $f_j : X \rightarrow Z_j$ . We generate the open cover  $\mathcal{U}_j = \{U_{ij}\}$  of  $Z_j$  as follows:

- (a) We divide each factor  $Z_j$  into  $n_j$  intervals (“sub-regions”), each of length  $\ell_j$ . Thus the entire  $d$ -dimensional region is divided into  $n_1 \times n_2 \times \dots \times n_m$  subregions, where each subregion represents a hyper-rectangle of area  $\ell_1 \times \ell_2 \times \dots \times \ell_m$ . Let the center of  $i^{\text{th}}$  hyper-rectangle be  $\{C_{1i}, C_{2i}, \dots, C_{mi}\}$ .
- (b) We fix the center of each hyper-rectangle, and increase the length along each factor  $Z_j$  by a certain percentage  $\alpha_j$  such that an overlapping region is created between consecutive pairs of the open sets  $U_{ij}$  and  $U_{i+1,j}$ , i.e.,  $U_{ij} \cap U_{i+1,j} \neq \emptyset$ . After increasing the length of all sides in this fashion, the new area of the hyper-rectangle is  $\ell_1(1 + \alpha_1) \times \dots \times \ell_m(1 + \alpha_m)^3$ . A 2D example is shown in Fig. 2.

We formulate the efficient determination of individual point sets belonging to each hyper-rectangle as a problem of range querying. Specifically, we implement the following querying function:

**Range Query:** *Given  $X$  and a hyper-rectangle  $h$ , return the subset of points in  $X$  that lie in  $h$ .*

To run this query efficiently, we use  $k$ -dimensional hyper-octrees [3, 11], which is a well known spatial data structure that uses recursive bisection to index a spatially distributed set of points. The compressed version of an  $n$ -leaves hyper-octree can be constructed in  $O(n \log n)$  time [3]. Once constructed, a balanced binary search tree that uses the order of the leaves is constructed. Using this auxiliary data structure, in combination with the hyper-octree, enables an  $O(\log n)$  worst case search time for both point and cell searches [3]. To answer the regional query for a hyper-rectangle  $h$ , we perform a top-down traversal of the hyper-octree by selectively retaining only those paths that can include at least one point within  $h$ . This can be achieved by keeping track of the corners of the cell defined by each internal node in the tree. This approach ensures that each such query can be answered in time that is bounded by the number of points in the hyper-rectangle.

## 2.2 Generation of Partial Clusters

Each open set (hyper-rectangle) computed by applying the filter functions is processed independently for generation of partial clusters. The goal of clustering is to partition the set of points in each hyper-rectangle based on their phenotypic performance.

Let  $U$  represent an open set of points  $\{x_1, x_2, \dots, x_t\}$ . Note that each point  $x \in U$  has a phenotypic trait value denoted by  $p(x)$ . We define a *distance function*  $d$  based on the phenotypic values of points in  $U$  as follows. Given two points with trait values  $p(x_i)$  and  $p(x_j)$ , the distance  $d(i, j) = |p(x_i) - p(x_j)|$ .

Given  $U$  and distance function  $d$ , a *partial clustering* is defined by a partitioning of the points in  $U$ . We denote the set of partial clusters resulting from any given open set  $U$  as  $\mathcal{C}_U$ . Subsequently, we denote the set of all partial clusters formed from *all* open sets (hyper-rectangles) by  $\mathcal{C} = \bigcup_U \mathcal{C}_U$ .

For the purpose of clustering, any distance-based clustering method can be applied. We implemented a density-based clustering approach very similar to that of DBSCAN [16]. In the interest of space, we omit details of our implementation. Of note are, however, two key points: a) the set of partial clusters generated from within a hyper-rectangle represents a partitioning of those points; and b) two partial clusters generated from a pair of adjacent (overlapping) hyper-rectangles could potentially have a non-empty intersection in points. In fact it is this intersection that renders connectivity among the partial clusters generated, the information for which will be used in the subsequent step of simplicial complex generation.

---

<sup>3</sup> See Section 2.4 for further explanation of how we choose the  $\alpha_i$  values.

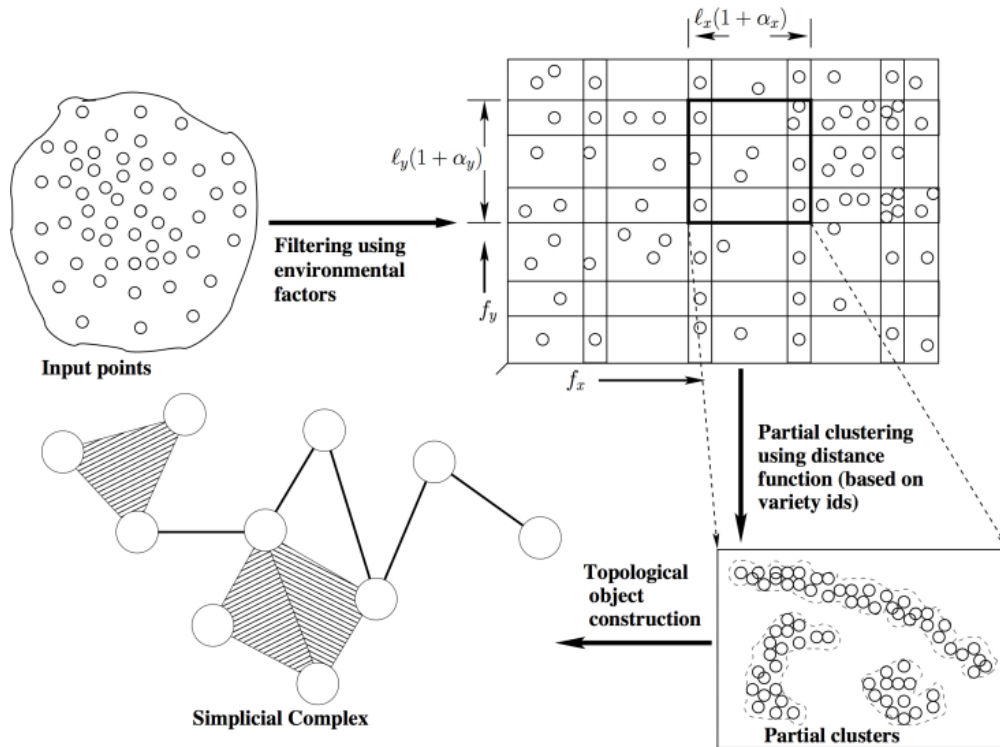


Figure 2: The TDA algorithmic framework for analyzing phenomic data.

### 2.3 Construction of Simplicial Complexes

From the set of partial clusters  $\mathcal{C}$ , we construct a simplicial complex  $K$  as follows. We describe the details for the 2D case, where no more than four open sets (hyper-rectangles) can mutually intersect. The extension to higher dimensions is straightforward. Starting with an empty simplicial complex, we implement the following steps:

- i) A 0-simplex (or vertex) is added to the simplicial complex  $K$  for every partial cluster.
- ii) Next, a 1-simplex (edge) is added to  $K$  for every non-empty 2-way intersection between any two partial clusters. Note that such intersections could exist only between partial clusters originating from different open sets.
- iii) Following the same procedure as above, we also add 2-simplices (triangles) and 3-simplices (tetrahedra) to  $K$  by enumerating only those 3-way and 4-way intersections, respectively, that could be non-empty.

The required multi-way intersections are computed using the range querying function described earlier (in Section 2.1).

### 2.4 Persistent homology

We employ the concept of persistent homology [15] to choose the final topological object for further analysis. In particular, the method in which overlapping intervals are chosen (by specifying growing overlap percentages  $\alpha_i$ , see Section 2.1) is already guided by this principle. Termed *multiscale mapper*, growing the intervals in this fashion ensures the topological objects formed (at each set of growing  $\alpha_i$  values) satisfy a monotonic inclusion property [13]. Hence results from persistent homology could be used to guarantee (theoretical) stability of the topological object formed (in the sense of persistence). At the same time, no implementation of multiscale mapper is known. Instead, we increase each  $\alpha_i$  in steps of 2.5%, and construct the topological objects for each set of  $\alpha_i$  values. We then construct the persistence barcodes (in dimensions 0, 1, and

2) using the sequence of topological objects formed by employing JavaPlex, a standard software tool for this purpose [2]. We then pick  $\alpha_i$ 's such that all three barcodes do not change for values at or higher than the chosen cutoff, ensuring the corresponding topological object chosen is indeed stable. This chosen topological object is analyzed further to identify interesting paths.

### 3 Interesting paths

The topological representation naturally reveals the underlying abstract structure of high-dimensional data. More specifically, a node (0-simplex) represents a partial cluster, which is a collection of points (i.e., a subpopulation) that shows similar phenotypic performance (by the distance function) under similar environmental conditions (filter intervals). An edge (1-simplex) connects two intersecting but distinct partial clusters. Therefore, by following a trail of nodes that show a monotonically varying performance, we can aim to capture the trail of subpopulations that gradually (or abruptly) alter their behavior under a continuously changing environment. Once identified, the user can extract points corresponding to these different subpopulations, and use them for comparative analyses and subsequent hypothesis extraction at the resolution of subpopulations.

Building on this idea, we formalize the notion of hypothesis extraction through exploration of topological objects as one of extracting “interesting paths” from the topological object. Details follow.

Using the simplicial complex  $K$ , we first construct a weighted directed acyclic graph  $G(V, E)$ , which represents the 1-skeleton of  $K$  along with some additional info. Let  $V(K)$  and  $E(K)$  denote the set of nodes and edges (0- and 1-simplices) of  $K$ . We set  $V = V(K)$  and  $E = E(K)$ .

Note that each node  $u \in V$  denotes a set of points that constitute a partial cluster in  $C$ . We denote this set as  $X(u)$ . Consequently, we assign real valued weights to all nodes and all edges in  $G$ —denoted by  $\omega(u)$  and  $\omega(e)$ , respectively, for  $u \in V$  and  $e \in E$ .

We set  $\omega(u)$  to be the average phenotypic value for all points in  $u$ :

$$\omega(u) = \frac{\sum_{x \in X(u)} p(x)}{|X(u)|}.$$

For an edge  $e = (u, v)$ , we assign as its weight the absolute difference between the weights of the two nodes:

$$\omega(e) = |\omega(v) - \omega(u)|.$$

In addition, the direction of an edge  $e$  is set from the lower weight node to the higher weight node—i.e., if  $\omega(u) \leq \omega(v)$ , then  $e : u \rightarrow v$ ; and  $e : v \rightarrow u$  otherwise.

**Edge and Path Definitions:** If the simplicial complex was constructed using  $k$  out of the  $m$  continuous variables (as filter functions), then along each edge, each continuous variable  $Z_i$  can independently increase or decrease. Since we are trying to link the change of each of these variables relative to the change in phenotype (along an edge), we record a  $k$ -bit *signature* for each edge.

The *signature* of an edge  $e \in E$  of  $G(V, E)$ , denoted by  $s(e)$ , is defined as a  $k$ -bit vector, where the  $i^{\text{th}}$  bit is 1 if the direction of change for the continuous variable  $Z_i$  is consistent with the direction of the edge, and 0 otherwise. In other words, let an edge's direction be  $u \rightarrow v$ . Then, if the mean value for the continuous variable  $Z_i$  increases from  $u$  to  $v$ , then the corresponding signature bit is 1; and 0 otherwise.

Fig. 3 illustrates a directed, signed edge in our representation.

Let  $P$  denote a directed path in  $G(V, E)$ , containing a sequence of  $r$  edges  $[e_1, e_2, \dots, e_r]$ . Path  $P$  is said to be *exact* if the signature of all edges along the path is identical; and *inexact* otherwise.

We define the *interestingness score*  $\mathcal{I}(P)$  of a path  $P$  as follows.

$$\mathcal{I}(P) = \sum_{i=1}^r \log(\text{rank}(e_i, P) + 1) \times \omega(e_i), \quad (1)$$

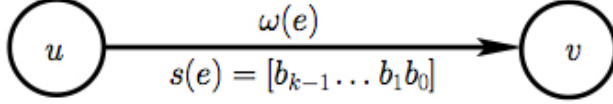


Figure 3: An edge  $e$  between two intersecting partial clusters (nodes  $u$  and  $v$ ). The direction of the edge indicates the direction in which the mean phenotypic/performance value increases. The signature  $s(e)$  is a  $k$ -bit vector that captures the directions of change for each of the  $k$  filter functions (e.g., environmental variables) along the edge—0 implies reducing and 1 implies increasing. The  $i^{\text{th}}$  bit corresponds to the  $i^{\text{th}}$  filter function.

where the  $\text{rank}(e, P)$  is the order of the edge  $e$  as it appears along the directed path  $P$ . Intuitively, we use the rank of an edge as an inflation factor for its weight—the later an edge appears in the path, the more its edge weight will count toward the interestingness of the path. This logic incentivizes the growth of long paths. The log function, on the other hand, helps contain this growth rate by treating edges that appear later in the path with comparable levels of importance (unless there is an order of magnitude increase in the path length).

We call two paths *overlapping* if they contain at least one edge in common.

**Finding a set of Interesting Paths ( $\mathcal{P}$ ) problem:** Given  $G(V, E)$  constructed as above, the goal is to *find a set of interesting paths*  $\mathcal{P} = \{P | P \in \mathcal{P}\}$  such that (i) no two paths are overlapped, and (ii) the total interestingness score of all paths  $\mathcal{I}(\mathcal{P}) = \sum_{P \in \mathcal{P}} \mathcal{I}(P)$  is maximized (over all choices of  $\mathcal{P}$ ).

### 3.1 The Algorithm

In this section, we present an efficient heuristic for the Interesting Paths problem. Our algorithm, while may not guarantee theoretical optimality in the interestingness score, runs in linear time (and space) and is effective in practice to identify meaningful paths with interesting aspects to them (as shown in Section 4). The main idea of our approach is to use dynamic programming.

Let  $e$  be an edge from  $u \rightarrow v$ . Then, we define the set of *candidate predecessor edges* for  $e$  as follows:

$$\text{Pred}(e) = \{f | f \in E, f : w \rightarrow u, \text{ such that } w \in V \text{ and } s(f) = s(e)\} \quad (2)$$

If the predecessor set is empty for an edge  $e$ , then the edge  $e$  is referred to as a *source edge*.

Let  $P_e$  denote an optimal path ending at edge  $e$ —i.e., a path with the maximum interestingness score ending at that edge. We compute two recurrences at edge  $e$ : i) the recurrence  $T(e)$  as the interestingness score of  $P_e$ ; and ii) a rank function  $\text{rank}(e)$  that stores the rank of  $e$  along the path  $P_e$ . The recurrences are as follows.

$$T(e) = \begin{cases} \omega(e), & \text{if } e \text{ is a source edge,} \\ T(f^*(e)) + \log(\text{rank}(f^*(e)) + 1) \times \omega(e), & \text{otherwise,} \end{cases} \quad (3)$$

where,  $f^*(e)$  is an *optimal predecessor* of  $e$ :

$$f^*(e) = \arg \max_f \{T(f) + \log(\text{rank}(f) + 1) \times \omega(e)\}. \quad (4)$$

Note that once  $T(e)$  is computed,  $\text{rank}(e)$  is given by:

$$\text{rank}(e) = \begin{cases} 2, & \text{if } e \text{ is a source edge,} \\ \text{rank}(f^*(e)) + 1, & \text{otherwise.} \end{cases} \quad (5)$$

A detailed pseudocode of our algorithm and a discussion on its runtime and memory complexities are provided in the Appendix (Section A).

## 4 Experimental Results

### 4.1 Experimental Setup

We tested our TDA framework on a real world maize data set. This data set consists of phenotypic and environmental measurements for two maize genotypes (abbreviated here for simplicity as  $A$  and  $B$ ), grown in two geographic locations (Nebraska (NE) and Kansas (KS)). The data consists of *daily* measurements of the genotype’s growth rate alongside multiple environmental variables, over the course of the entire growing season (100 days). For the purpose of our analysis we treat each “point” to refer to a unique [genotype, location, time] combination. Consequently, the above data set consists of 400 points ( $n$ ). Here, “time” was measured in the Days After Planting (DAP).

Each point has one phenotypic value (growth rate) and 10 environmental variables (including but not limited to: humidity, temperature, rainfall, solar radiation, soil moisture, soil temperature). For the purpose of the studies presented in this paper, we select humidity, temperature and solar radiation, as they were the top variables that showed the most interesting trends and observations against the phenotypic trait. Results for other variables are omitted due to space considerations.

### 4.2 Topological object construction

We tested our framework using both single and two filter function(s).

**Single filter function:** The goal of our single filter study was to understand how the [location, genotype] combinations showed different performance in the phenotype as a function of time. Consequently, we used DAP as the filter function<sup>4</sup> and built our topological object, as described in Section 2.

Fig. 4 shows the resulting topological object. As can be seen, our method demonstrates the ability to clearly separate the two genotypes in both locations—as seen in the branching of paths, and the branch points in time indicate the DAP at which those genotypes separate. Notably, in both KS and NE, genotype B shows an accelerated growth rate earlier in its developmental stage than for A. Furthermore, both varieties in KS show an accelerated growth rate earlier than their NE counterparts. These observations are also confirmed by the scatter plot (Fig. A1 in the Appendix).

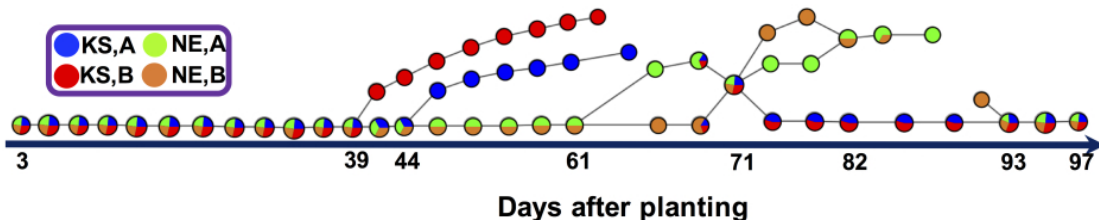


Figure 4: Topological object based on the single filter function of days after planting (DAP). Here we considered both genotypes ( $A$  and  $B$ ) in both locations (KS and NE). The pie chart at each node indicates the relative frequency of the four [location, genotype] combinations.

**Two filter functions:** While the above single filter function study shows some interesting behavioral differences between the genotypes with time and location, it is not adequate to provide any clues on the *basis* for such differences. In fact, what led to genotype B behaving differently across the two different locations? To delve into this specific question further, we

<sup>4</sup> The topological objects resulting from the use of other variables such as humidity and solar radiation as the single filter function are shown in the Appendix (Section B).



include a second filter function, which can be any one of the environmental variables<sup>5</sup>, and include only the genotype B points (i.e., [KS,B] and [NE,B]) for subsequent analysis. Fig. 5 shows the topological object generated using DAP and humidity as the two filter functions.

The topological object contains two large connected components. In the topological object colored by mean DAP (Fig. 5(C)), we notice that the largest connected component (right-top) captures the points from early to active growth stages, whereas the other connected component (left-bottom) holds the points for the post-growth stage (DAP roughly over 70).

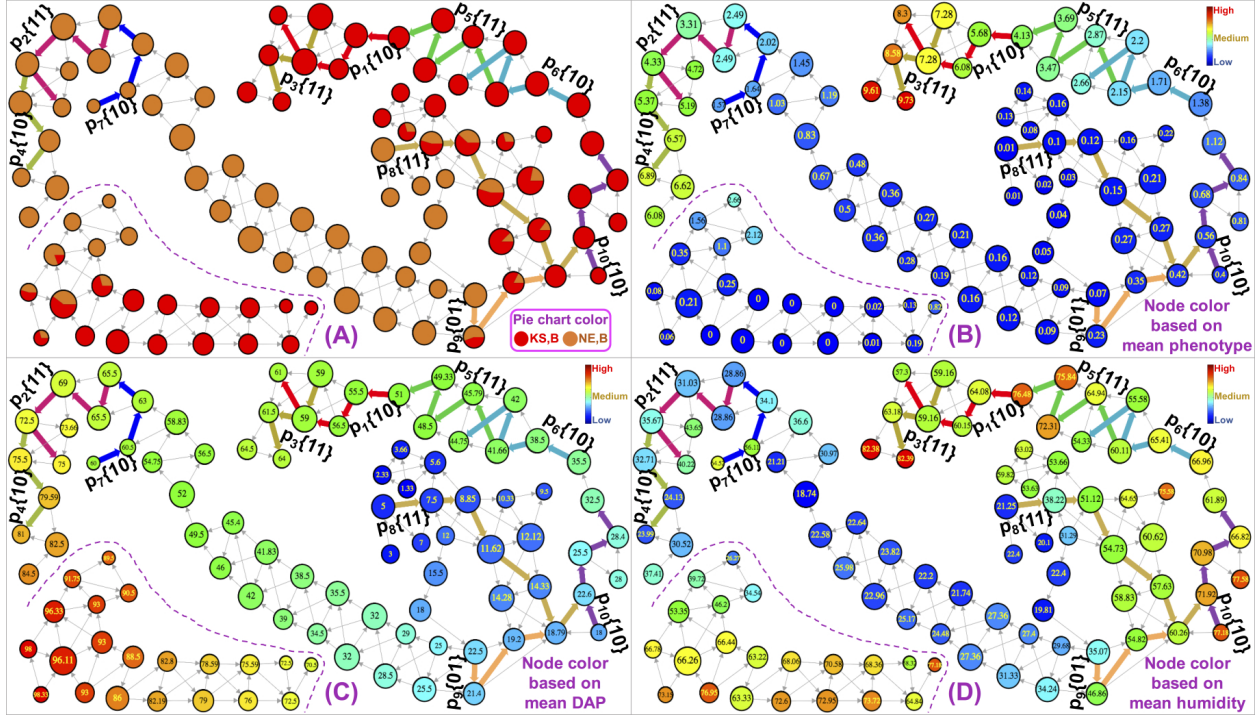


Figure 5: The topological object constructed using DAP and humidity as the two filter functions, using only the [KS,B] and [NE,B] points. The same object is shown in the four panes, albeit with different coloring schemes. (A) shows each node (i.e., partial cluster) as a pie-chart of the relative concentrations of the two possible [location,genotype] combinations; (B) shows nodes colored by their mean phenotypic value; (C) shows nodes colored by their mean DAP value; and (D) shows nodes colored by their mean humidity value. The mean values are also indicated within the respective circles. The size of the circle for each node is proportional to the size of the corresponding partial cluster. Also shown highlighted as thick colored edges are the set of interesting paths identified by our method. Edge directions are from low to high mean phenotypic values. The interesting paths are labeled as  $P_i\{s_1s_2\}$ , where  $i$  is the path number, and  $s_1s_2$  denotes the signature for that path ( $s_1$  corresponds to DAP and  $s_2$  corresponds to humidity). Recall that in the signature, 0 means decreasing and 1 means increasing.

<sup>5</sup> Section C.1 in the Appendix shows the results for an alternative setup where the two filter functions used are two environmental variables.

### 4.3 Path analysis

As our next step, we identified multiple interesting paths from the topological object constructed using DAP and humidity as the two filter functions, using the method described in Section 3. Fig. 5 shows (using different colors) the paths that were automatically detected. For the purpose of this analysis, we kept the signature along a path fixed<sup>6</sup>.

We now evaluate the qualitative significance of the interesting paths identified by our method, shown in Fig. 5:

- The collection of co-located paths  $P_8, P_9, P_{10}$  essentially helps us understand how the genotype behaves in its early stages of development, in the two locations. More specifically, path  $P_8$  starts with points from both locations because their performances in similar conditions (DAP and humidity) are also very similar; however, after roughly 20 DAP (Fig. 5C), the points from KS and NE separate (into  $P_{10}$  and  $P_9$  respectively).
- The sequence of paths  $[P_6, P_5, P_1, P_3]$ , which also includes the *most* interesting path by interestingness score ( $P_1$ ), represents the active growth period for the KS population (see Fig. 5B). In this period, the growth rate increased from 1.38 cm/DAP to 9.73 cm/DAP, from approximately 35 DAP to 64 DAP (see Fig. 5C). In contrast, the plants in NE, despite being the same genotype, had very low growth rates during roughly the same period in time (35 DAP to 55 DAP; see Figs. 5B, 5C).

Incidentally, examining the humidity trends in the same period for these two locations (see Fig. 5D), we see that the humidity was very low in NE compared to KS, and that the increase in humidity values for the NE population (after 58 DAP) coincides with the increased activity in its growth rate (see Figs. 5C, 5D)—thereby giving us an indicator that humidity may have an active role in NE, perhaps more so than in KS, in accelerating growth rate during the mid-stages of development.

- The sequence of paths  $[P_7, P_2, P_4]$  represents the active growth period of the NE population, where the growth rate increases from 1.57 cm/DAP to 6.89 cm/DAP (Fig. 5B). This high activity period starts from approximately 60 DAP and ends roughly at 81 DAP. As indicated above, this active growth rate coincides with the period with higher humidity for NE.

To better understand the results and contrast it with more traditional approaches, we plotted all the genotype B points as a scatter plot, based on their DAP and humidity—see Fig. 6. The coloring of the points are by their location. As can be seen, the plot shows a clear separation between NE and KS humidity values, with NE exposed to lower humidity values than KS, in general. However, this is coarse-level information which can be easily obtained through a correlation test as well. At the same time, such tests are *not* adequate to provide meaningful insights into where the environmental or temporal triggers are relative to the performance, and how that behavior varies within a diverse population. That is where our topology-based approach can be useful—to make such inferences from the data and formulate testable hypothesis.

To better illustrate this advantage, we overlaid the interesting path sequences identified by our paths (discussed above) on to the scatter plot. These path sequences are shown as arcs in Fig. 6. As can be seen, our interesting paths show three major “features” within this scatter plot:

- i) the initial sequence where both NE and KS varieties behave similarly in their initial developmental stages, before branching out (around 20 DAP);
- ii) the period of active growth for [KS,B] between roughly 35 and 65 DAP; and
- iii) the period of active growth for [NE,B] appearing much later, between roughly 60 and 85 DAP.

More interestingly, the beginning of our interesting paths for [NE,B] is also for the first time the humidity value experienced a spike for that location—increasing from values under 30 to around 60s—effectively implying (or at least indicating) a probable cause for increased growth activity.

---

<sup>6</sup>Our method has a feature to relax this condition, and we performed more analysis using that feature (not reported due to space). Of note is that the paths tend to get longer with this relaxation.

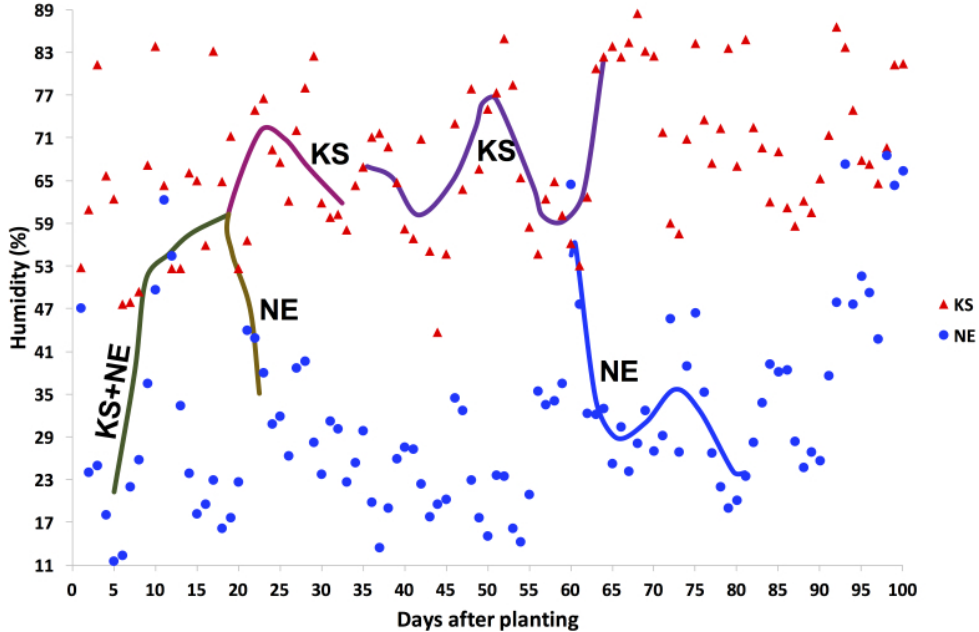


Figure 6: Scatter plot of data points ([individual, date/time]) with respect to DAP and humidity in both locations. The color of a point indicates the corresponding location. According to this figure, the range of humidity is higher in KS compared to NE. The paths generated from our TDA framework are overlaid in this figure, which illustrate the phenotypic information.

After that trigger, minor fluctuations in humidity seemed to have little effect in the growth rate, which continued to increase through DAP 85. This study sets up a testable link between a genotype (B) and environmental variable (in this case, humidity) toward a performance trait (growth rate). Furthermore, the study raises a plausible working hypothesis that can be tested: “If genotype [NE,B] is also exposed to a higher level humidity earlier on, during its developmental stage, then it is also likely to show an active growth rate earlier?”

This illustrative example serves to demonstrate that our topology-based method also has the potential to enrich the information over what can be obtained through only conventional methods such as scatter plots. Note that our tool is meant for exploring high-dimensional data in a software-guided manner and more/other environmental variables can be included in our tests. In fact, in the Appendix, we present more studies along this line by replacing humidity with temperature and solar radiation.

Our study about the impact of temperature on plant growth rate is presented in Appendix in Section C.2.

## 5 Related work

We are not aware of any previous automated or semi-automated hypothesis extraction approaches for high-dimensional data sets.

**Topology and Applications:** There are several important properties that make algebraic topology particularly effective for gleaning structural features out of high-dimensional data. First, topology studies shapes in a *coordinate-free way*, which enables comparison among data sets from diverse sources or coordinate systems. Second, topological constructions are *not sensitive to small changes in data*, and robust against noise. Third, topology works with *compressed representations* of spaces in the form of *simplicial complexes* (or triangulations) [22], which

preserve information relevant to how points are connected. Compared to more traditional techniques such as principal component analysis, multidimensional scaling, manifold learning, and cluster analysis, topological methods are known to be more sensitive to both large and small scale patterns [20].

Topological data analysis (TDA) has been applied to a wide range of application domains, albeit for mostly visualization purposes [12, 10, 5, 14, 18, 23, 26]. The foundational work in TDA most relevant to this paper was done by Carlsson and coworkers [20]. In [25], they describe a framework called *Mapper* to model and visualize high-dimensional data. Most of this work has been on the visualization front. A topology-based approach was also rated as the best overall entry at an expression QTL (eQTL) visualization competition organized by the BioVis community [6].

**Tools for Plant Phenomics:** Tools to decode associations between genotypes and phenotypes have been under development for over two decades. These tools look at the genetic variation observed at one or more loci along the genome and study their correlation to quantitative traits. The techniques used can be summarized as follows: i) Linkage mapping techniques that use prior knowledge on the location (markers) responsible for a certain trait; ii) Quantitative Trait Locus (QTL) mapping that extends linkage to an interval of co-located markers along the genome; and iii) Genome-Wide Association Studies (GWAS), which takes a whole genome approach by scoring multiple markers located across the genome for specific traits. In relation to capturing environmental variability, efforts have been sparse. [8] presented an experimental framework supplemented by GWAS to model environmental effects on phenotypes. [19] provided a generalized linear model-based method to capture gene to environment interactions.

## 6 Conclusion

We have presented a scalable exploratory framework for navigating high-dimensional data sets and applied it to plant phenomics data to analyze the effect of environmental factors on phenotypic traits. At its core, our approach is fundamentally different from state-of-the-art techniques in many ways: First, it inherits the advantages of topology including its use of a coordinate-free representation, robustness to noise, and natural rendition to compact representations. Second, by allowing the user to define multiple filter functions, it enables them to study the combined effect of multiple factors on target performance traits. Third, through its clustering and visualization capabilities, it provides a way for domain experts to readily observe emergent behavior among different groups or subpopulations without requiring the knowledge of any priors. This feature enables scientists to identify subpopulations, compare them, and perform more targeted studies to formulate and test hypotheses.

Our approach is scalable in that it can scale to large data sets containing possibly tens of thousands of points, reducing such large data to tens or hundreds of partial clusters, thereby making visualization and exploration possible. Although we have presented results on a smaller data set, we have tested our approach on larger data sets (e.g., with thousands of points [1]; we did not present these results due to space constraints and also due to some missing information about the data (e.g., genotypes)).

While the scope of this work can be further expanded through application to a broader range of phenomics data collections, the results presented in this paper show a promising application of topology and its role in hypothesis extraction from high-dimensional data sets. Considering the nascency of the phenomics field, tools for users to explore data and help extract plausible hypothesis in a data-guided manner from large-scale complex data, will be important going forward.

**Acknowledgements:** We are grateful to Colton McNinch who contributed to the data collection.

This research was in part supported by U.S. National Science Foundation (NSF) grants DBI 1661348, AF 1064600, and U.S. Department of Energy (DOE) grant DE-SC-0006516.

## References

- [1] Syngenta crop challenge in analytics. <https://www.ideaconnection.com/syngenta-crop-challenge/challenge.php>. [Last; accessed January-2016].
- [2] ADAMS, H., TAUSZ, A., AND VEJDEMO-JOHANSSON, M. javaPlex: A Research Software Package for Persistent (Co)Homology. In *Mathematical Software ICMS 2014*, H. Hong and C. Yap, Eds., vol. 8592 of *Lecture Notes in Computer Science*. Springer Berlin Heidelberg, 2014, pp. 129–136. Software available at <http://git.appliedtopology.org/javaplex/>.
- [3] ALURU, S., AND SEVILGEN, F. E. Dynamic compressed hyperoctrees with application to the n-body problem. In *Foundations of Software Technology and Theoretical Computer Science* (1999), Springer, pp. 21–33.
- [4] ASPB, R. Unleashing a decade of innovation in plant science: A vision for 2015-2025. Plant Science Research Summit, 2013.
- [5] BAN, Y.-E. A., EDELSBRUNNER, H., AND RUDOLPH, J. Interface surfaces for protein-protein complexes. *Journal of the Association for Computing Machinery* 53, 3 (2006), 361–378.
- [6] BARTLETT, C. W., CHEONG, S. Y., HOU, L., PAQUETTE, J., LUM, P. Y., JGER, G., BATTKE, F., VEHLow, C., HEINRICH, J., AND NIESELT, K. An eQTL biological data visualization challenge and approaches from the visualization community. *BMC bioinformatics* 13, Suppl 8 (2012), S8. 00005.
- [7] BILDER, R. M., SABB, F., CANNON, T., LONDON, E., JENTSCH, J., PARKER, D. S., POLDRACK, R., EVANS, C., AND FREIMER, N. Phenomics: the systematic study of phenotypes on a genome-wide scale. *Neuroscience* 164, 1 (2009), 30–42.
- [8] BROWN, T. B., CHENG, R., SIRAUlt, X. R., RUNGRAT, T., MURRAY, K. D., TRTILEK, M., FURBANK, R. T., BADGER, M., POGSON, B. J., AND BOREVITZ, J. O. TraitCapture: genomic and environment modelling of plant phenomic data. *Current opinion in plant biology* 18 (2014), 73–79.
- [9] CARLSSON, G. Topology and data. *Bulletin of the American Mathematical Society* 46, 2 (Jan. 2009), 255–308.
- [10] CARLSSON, G., ZOMORODIAN, A., COLLINS, A., AND GUIBAS, L. Persistence barcodes for shapes. In *Proceedings of the 2004 Eurographics/ACM SIGGRAPH symposium on Geometry processing* (New York, NY, USA, 2004), SGP '04, ACM, pp. 124–135.
- [11] CLARKSON, K. L. Fast algorithms for the all nearest neighbors problem. In *Foundations of Computer Science, 1983., 24th Annual Symposium on* (1983), IEEE, pp. 226–232.
- [12] DE SILVA, V., AND GHRIST, R. Coverage in sensor networks via persistent homology. *Algebraic and Geometric Topology* 7 (2007), 339–358.
- [13] DEY, T. K., MÉMOLI, F., AND WANG, Y. Multiscale mapper: Topological summarization via codomain covers. In *Proceedings of the Twenty-Seventh Annual ACM-SIAM Symposium on Discrete Algorithms* (Philadelphia, PA, USA, 2016), SODA '16, Society for Industrial and Applied Mathematics, pp. 997–1013.
- [14] EDELSBRUNNER, H., AND KOEHL, P. The geometry of biomolecular solvation. In *Combinatorial and Computational Geometry* (2005), vol. 52 of *MSRI Publications*, pp. 243–275.
- [15] EDELSBRUNNER, H., LETSCHER, D., AND ZOMORODIAN, A. Topological persistence and simplification. *Discrete and Computational Geometry* 28 (2002), 511–533.
- [16] ESTER, M., KRIEGEL, H.-P., SANDER, J., AND XU, X. A density-based algorithm for discovering clusters in large spatial databases with noise. In *KDD* (1996), vol. 96, pp. 226–231.
- [17] HOULE, D., GOVINDARAJU, D. R., AND OMHOLT, S. Phenomics: the next challenge. *Nature Reviews Genetics* 11, 12 (2010), 855–866.

- [18] HUAN, J., BANDYOPADHYAY, D., WANG, W., SNOEYINK, J., PRINS, J., AND TROPSHA, A. Comparing graph representations of protein structure for mining family-specific residue-based packing motifs. *Journal of Computational Biology* 12, 6 (2005), 657–671.
- [19] LOU, X.-Y., CHEN, G.-B., YAN, L., MA, J. Z., ZHU, J., ELSTON, R. C., AND LI, M. D. A generalized combinatorial approach for detecting gene-by-gene and gene-by-environment interactions with application to nicotine dependence. *The American Journal of Human Genetics* 80, 6 (2007), 1125–1137.
- [20] LUM, P. Y., SINGH, G., LEHMAN, A., ISHKANOV, T., VEJDEMO-JOHANSSON, M., ALAGAPPAN, M., CARLSSON, J. G., AND CARLSSON, G. Extracting insights from the shape of complex data using topology. *Scientific Reports* 3, 1236 (2013).
- [21] MARTIN, C. The plant science decadal vision. *The Plant Cell Online* 25, 12 (2013), 4773–4774.
- [22] MUNKRES, J. R. *Elements of Algebraic Topology*. Addison–Wesley Publishing Company, Menlo Park, 1984.
- [23] NICOLAU, M., LEVINE, A. J., AND CARLSSON, G. Topology based data analysis identifies a subgroup of breast cancers with a unique mutational profile and excellent survival. *Proceedings of the National Academy of Sciences* 108, 17 (2011), 7265–7270.
- [24] NIFA-NSF. Phenomics: Genotype to Phenotype. NIFA - NSF Phenomics Workshop Report, 2011.
- [25] SINGH, G., MEMOLI, F., AND CARLSSON, G. Topological Methods for the Analysis of High Dimensional Data Sets and 3D Object Recognition. In *Proceedings of the Symposium on Point Based Graphics* (Prague, Czech Republic, 2007), M. Botsch, R. Pajarola, B. Chen, and M. Zwicker, Eds., Eurographics Association, pp. 91–100.
- [26] VAN DE WEYGAERT, R., VEGTER, G., EDELSBRUNNER, H., JONES, B. J., PRANAV, P., PARK, C., HELLOWING, W. A., ELDERING, B., KRUTHOF, N., BOS, E. P., HIDDING, J., FELDBRUGGE, J., TEN HAVE, E., VAN ENGELEN, M., CAROLI, M., AND TEILLAUD, M. Alpha, betti and the megaparsec universe: On the topology of the cosmic web. In *Transactions on Computational Science XIV*, M. Gavrilova, C. Tan, and M. Mostafavi, Eds., vol. 6970 of *Lecture Notes in Computer Science*. Springer Berlin Heidelberg, 2011, pp. 60–101.

# Appendix

## A Algorithm

---

**Algorithm 1:** Finding interesting paths from a Topological object (Graph G)

---

**input :** Directed acyclic graph  $G = (V, E)$  with edge weight  $\omega$  and *rank*

**output:** A set of interesting paths,  $\mathcal{P}$

**begin**

$R$ : Set of nodes (“roots”) with no incoming edges

$\Gamma(u) = \{v \mid (u, v) \in E\}, \forall u, v \in V$

$s(e)$ : Signature of edge  $e$

$\Phi(e) = \{e_1 \mid e_1 \in E, \exists u, v, w \in V, v \in \Gamma(u), w \in \Gamma(v), e \leftarrow (u, v), e_1 \leftarrow (v, w), s(e) = s(e_1)\}$

$P \leftarrow \emptyset$  // The set of nodes of an interesting path enumerated so far

$\mathcal{P} \leftarrow \emptyset$  // The set of interesting paths enumerated so far

$\mathcal{L} \leftarrow \emptyset$  // The set of terminal edges for all interesting paths enumerated so far

$Q \leftarrow \emptyset$  // Queue for the next batch of nodes to be processed

**Step 1. Initialization**

**foreach**  $u \in R$  **do**

**foreach**  $v \in \Gamma(u)$  **do**

        Let,  $e \leftarrow (u, v)$

        Initialize *rank*( $e$ ) and weight  $\omega(e)$

$T(e) \leftarrow \omega(e)$

$Enqueue(Q, v)$

**Step 2. Computing recurrence at every edge**

**while**  $Q \neq \emptyset$  **do**

$u = Dequeue(Q)$

**foreach**  $v \in \Gamma(u)$  **do**

        Let,  $e \leftarrow (u, v)$

        edge  $\hat{e} = f^*(e)$ , an optimal predecessor of  $e$

**if**  $\hat{e} \neq NULL$  **then**

            Compute  $T(e)$  and *rank*( $e$ ) using  $\hat{e}$

**else**

            Initialize *rank*( $e$ ) and weight  $\omega(e)$

$T(e) \leftarrow \omega(e)$

$Enqueue(Q, v)$

**if**  $\Phi(e) = \emptyset$  **then**

$\mathcal{L} \leftarrow \mathcal{L} \cup \{e\}$

**Step 3. Back tracking for path enumeration**

Sort the edges of set  $\mathcal{L}$  in descending order based on their scores

**foreach**  $e \in \mathcal{L}$  **do**

    Retrieve all the nodes along a non-overlapping path that terminates at edge  $e$

    Add all the nodes to  $P$

$\mathcal{P} \leftarrow \mathcal{P} \cup P$

$P \leftarrow \emptyset$

**return**  $\mathcal{P}$

---

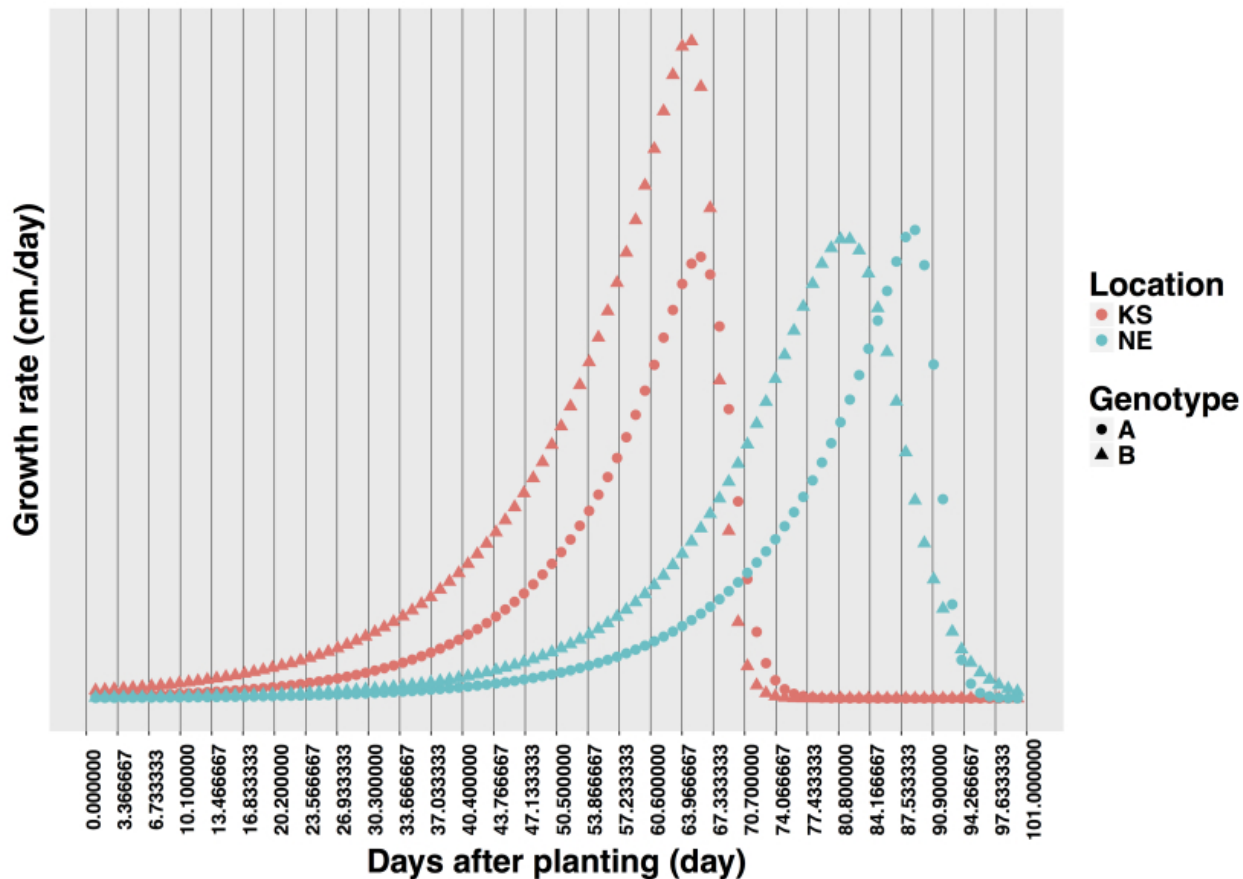


Figure A1: The scatter plot of growth rate with respect to days after planting (DAP). Plants started to grow earlier in location KS compared to location NE. Genotype *B* of location KS acts differently compared to both genotypes in both locations.

### A.1 Complexity analysis

Let, for a given DAG  $G = (V, E)$ ,  $n$  is the number of nodes ( $|V|$ ) and  $m$  is the number of edges ( $|E|$ ). Also let,  $m_{\mathcal{L}}$  is the cardinality of set  $\mathcal{L}$ .

**Time complexity:** The above algorithm visited every edge at most twice during forward computation (Step 1 and Step 2) and a subset of edges visited again during backward computation (Step 3). In total (Step 1, Step 2 and Step 3) an edge visited at most thrice. The frequency to visit a node is equal to the number of incoming edges of that node. Hence, the time complexity is  $O(n + m)$ . However, theoretically the sorting step (start of Step 3) has a worst case complexity of  $m_{\mathcal{L}} \log(m_{\mathcal{L}})$  but in practice, we observed that  $m_{\mathcal{L}} \ll m$ . Therefore,  $m_{\mathcal{L}} \log(m_{\mathcal{L}})$  will not be a dominating term in the overall time complexity  $O(n + m)$ .

**Space complexity:** In terms of space (memory), our algorithm stores all the nodes and edges of a given DAG  $G$ . Therefore, the space complexity is  $O(n + m)$ .

## B Single filter function

Fig. A2 shows the resulting topological object constructed using humidity as a single filter function. As can be seen, our method demonstrates the ability to very clearly separate the two locations (NE and KS)—this can be seen in the form of two graphs where one graph contains



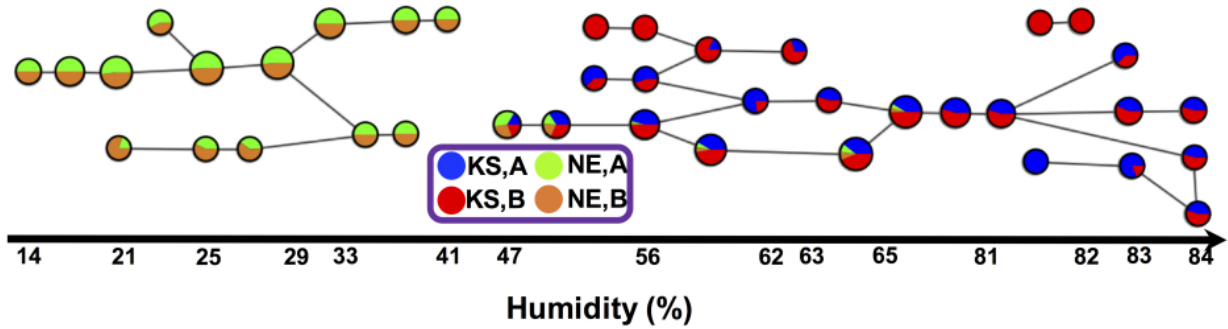


Figure A2: Topological object based on single filter function of humidity. The pie chart at each node indicates the cardinality under a certain individual ( $j$ genotype, $location_j$ ).

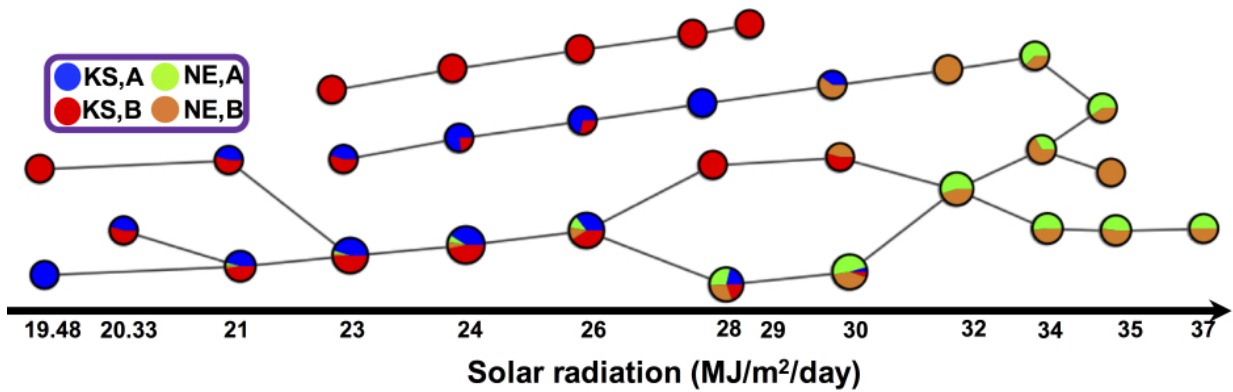


Figure A3: Topological object based on single filter function of solar radiation. The pie chart at each node indicates the cardinality under a certain individual ( $j$ genotype, $location_j$ ).

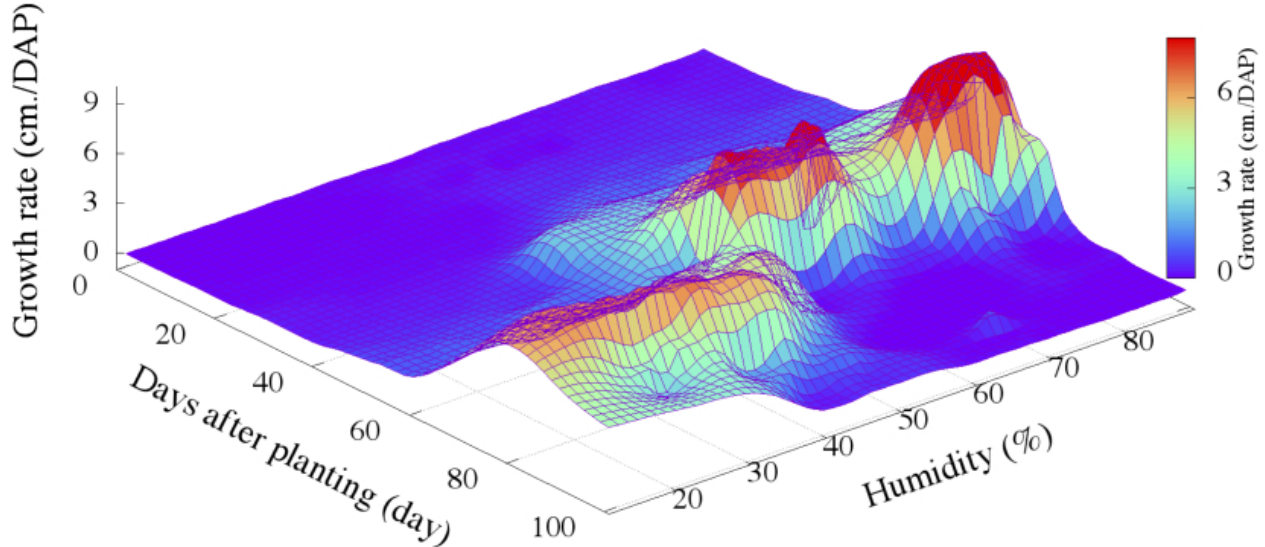


Figure A4: 3D representation of phenotype (growth rate) data with respect to time (DAP) and one of the environmental attributes (Humidity) for a real-world maize data set grown in Kansas (KS) and Nebraska (NE). Each point in the landscape is a [genotype,location,date/time] combination.

the genotypes of NE and the other graph mostly contains the genotypes of location KS.

The topological object constructed using solar radiation as a single filter function shows at Fig. A3. Our method demonstrates the ability to detect genotype *B* acts differently from genotype *A* under the same range of solar radiation ( $23 - 29 MJm^{-2}day^{-1}$ ) in KS.

## C Double filter function

### C.1 DAP and humidity

The landscape view of Fig. A4 shows the change of phenotypic value with respect to both time (DAP) and environment (humidity). While some general trends might be evident from this visualization, the question of which subset of points should be compared to which others in order to discern the independent or combined effects of time and environment cannot be answered easily, due to the explosive number of such combinations. In order to delineate the phenotypic variation of a subpopulation under certain environmental condition over a period, we applied topological data analysis methodology. The step by step construction process of our topological object using DAP and humidity as the double filter function are as follows:

#### C.1.1 Filtering

The scatter plot of Fig. 6 shows the data points ([genotype,location,date/time]) with respect to two filters, one is time (DAP) and other is environment (humidity). We created 30 windows along the filter DAP and 5 windows along the filter humidity, which creates 150 rectangular interval. Each rectangle has a center point. Initially we did not have any overlapping between two adjacent rectangles. We started from 2.5% overlapping between two adjacent rectangles by increasing the length of each rectangle along both sides from the center point of corresponding rectangle.

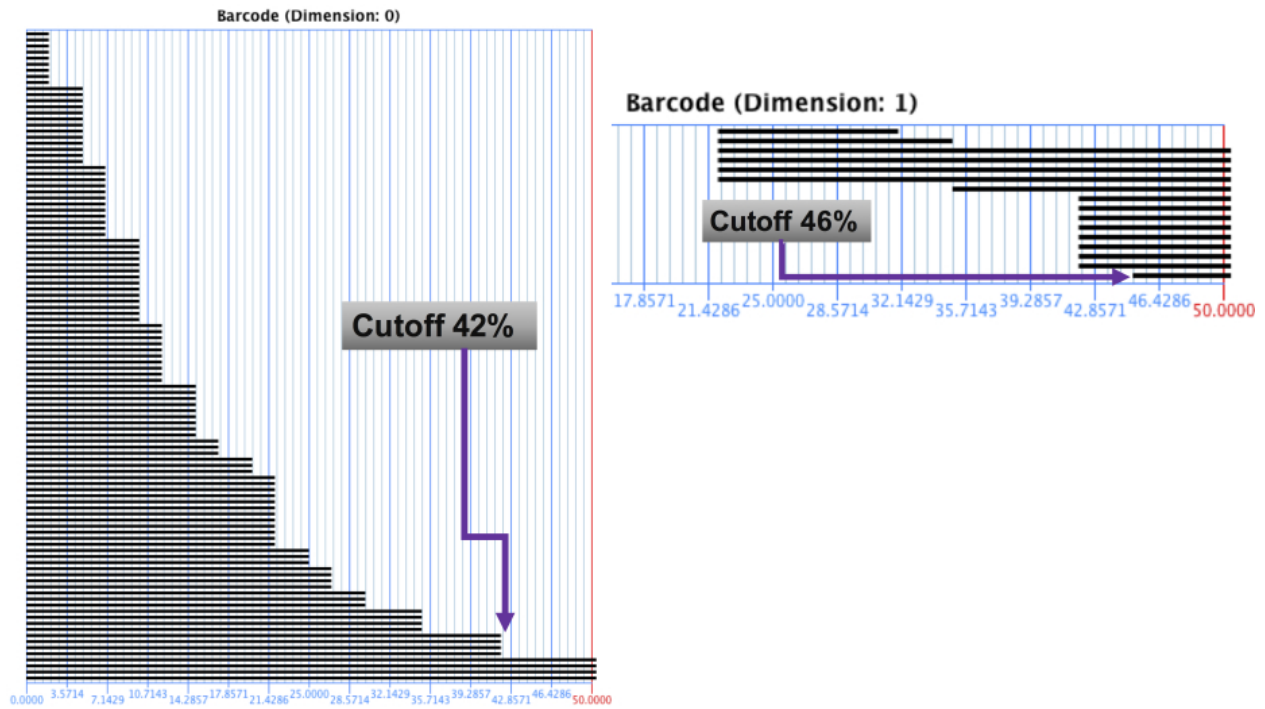


Figure A5: Barcode generated from 0% overlapping to 50% overlapping with 2.5% interval. Barcode of ‘dimension 0’ shows the number of connected components and barcode of ‘dimension 1’ indicates the number of holes. Each horizontal bar specifies the life span of a simplex in terms of percentage overlapping value. The percentage overlapping value after which there has no any terminal point of any simplex is considered as the persistent value. Here, the number of connected components are not changing after 42% and the number of holes are not changing after 46%. These two values are the persistent values and we chose the larger one.

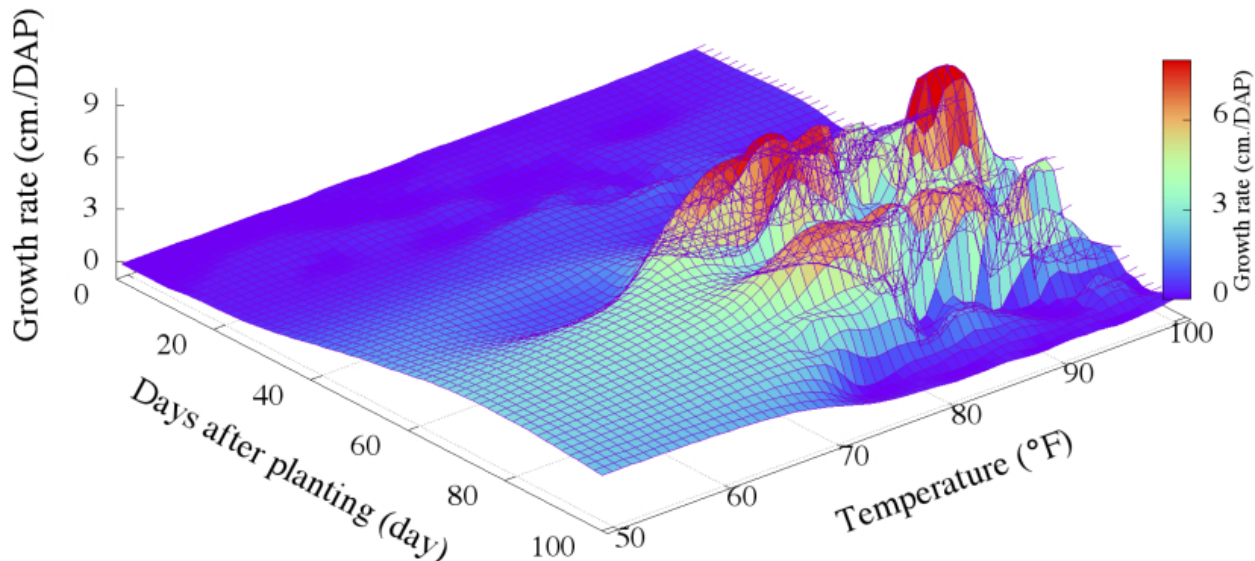


Figure A6: 3D representation of phenotype (growth rate) data with respect to time (Days after planting) and one of the environmental attributes (Temperature) for a real-world maize data set grown in Kansas (KS) and Nebraska (NE). Each point in the landscape is a [genotype,location,date/time] combination.

### C.1.2 Partial clusters

In the next step to compute partial clusters, the point set from each rectangular interval was clustered using the algorithm described in main paper (Section 2.2). The *distance* between any two points in the set was given by the absolute difference of their trait values. Using the density-based clustering algorithm (see Section 2.2), we generated a set of partial clusters for every rectangular interval. Every rectangular interval contains a set of points. We calculated standard deviation of phenotypic values for all the points in a rectangle. The mean value of all the standard deviations is used as a clustering radius, which is  $r = 0.7$  for this experiment. The density threshold of the clustering is  $\rho = 2$ , which is fixed in our experiments.

### C.1.3 Simplicial complex

The output of our TDA framework is a simplicial complex constructed using the overlaps among the set of partial clusters generated from all rectangular intervals. Recall that each node represents a partial cluster. In our visual representation of the complex, the size of each node is scaled to its weighted cardinality (as defined by the number of core and peripheral points within that cluster).

### C.1.4 Persistent homology

As a process to apply homology, which is described in section 2.4 of main paper, we generated a set of overlapping parameters started from 2.5% to 50% with 2.5% interval. For each overlapping parameter, when a simplicial complex generated, we recorded all the new simplex information against that overlapping value. This overlapping value is considered as a birth or starting point of that new simplex. Similarly, when any existing simplex is replaced by a new simplex (i.e. 1-simplex can be replaced by 2-simplex when a new cluster overlaps two existing clusters of 1-simplex) then that overlapping value is considered as the death or terminating point for the old simplex as well as the birth point for new simplex. After generating simplicial complexes

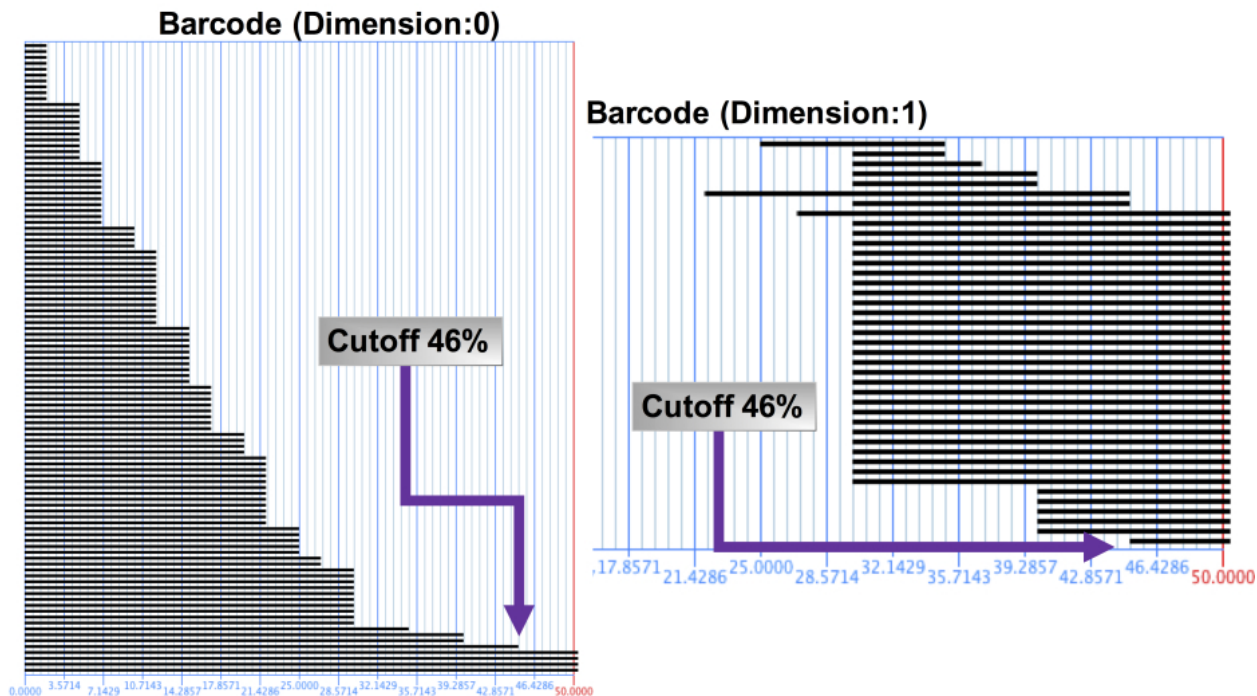


Figure A7: Barcode generated from 0% overlapping to 50% overlapping with 2.5% interval. Both the number of connected components and holds are not changing after 46% overlapping which is considered as the persistent value.

for all the overlapping parameters, we got a list of birth and dead overlapping values of the simplices. This record is used to generate barcode.

Recall from section 2.4, barcode for dimension *zero* indicates the number of connected components and barcode for dimension *one* indicates the number of holes. The barcodes generated from our dataset (Fig. A5) shows that the number of connected components did not change after 42% and the number of holes did not change after 46%. We considered 46% as a constant overlapping value for this double filter function (DAP and Humidity).

### C.1.5 Topological object

The topological object in Fig. 5 was generated considering the 46% overlapping. The details analysis of this object is in the result section of the main paper.

## C.2 DAP and temperature

The landscape view of Fig. A6 shows the change of phenotypic value with respect to both time (DAP) and on of the environment attributes (temperature). We followed the same construction process discussed in section C.1 to generate the topological object using double filter function (DAP and temperature). For this double filter function, we used 46% overlapping (Fig. A7) and  $r = 0.6$  as the clustering radius.

### C.2.1 Topological object

The topological object in Fig. A8 generated considering 46% overlapping. Here, each node is a cluster that contains a set of points, where each point is a collection of individuals. In order to visualize the cardinality of a specific individual in a node, we plotted each node as a pie chart.

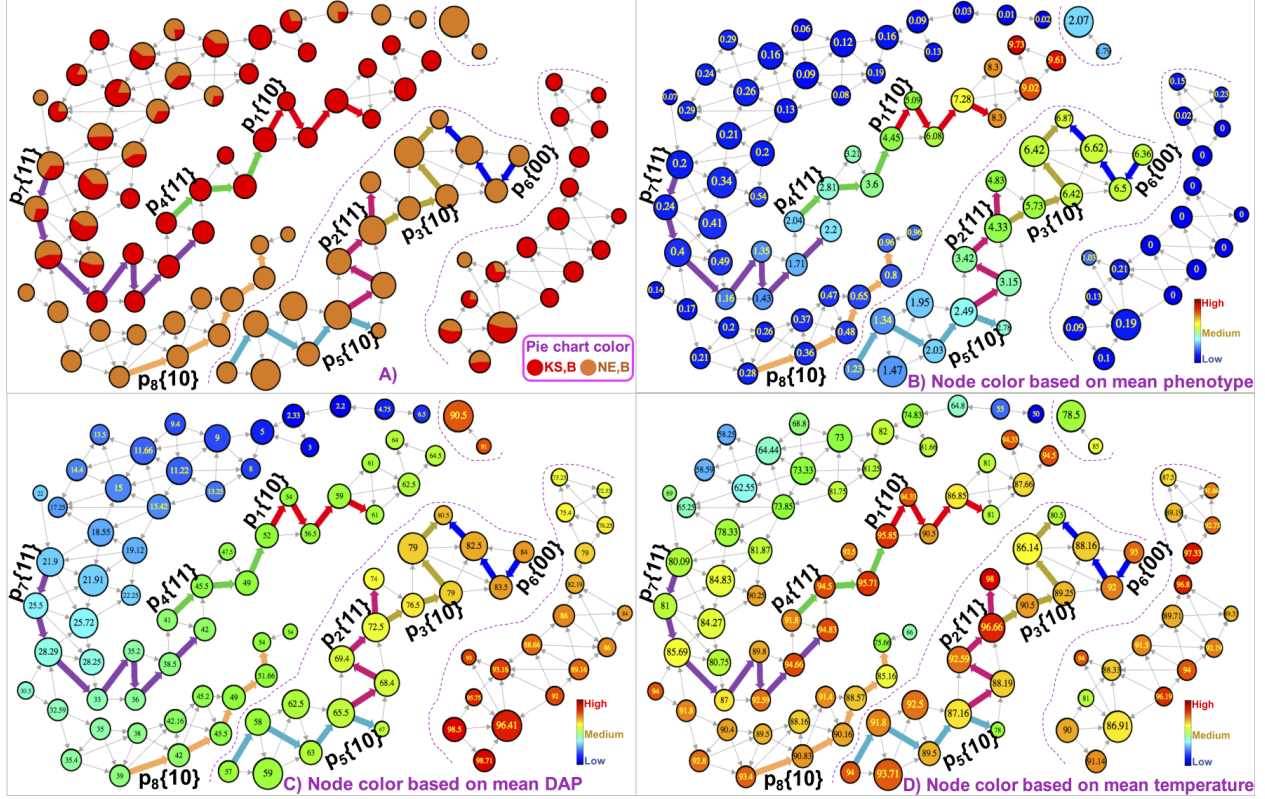


Figure A8: The topological object constructed using DAP and temperature as the double filter function, using only the [KS,B] and [NE,B] points. The same object is shown in the four panes, albeit with different coloring schemes. (A) shows each node (i.e., partial cluster) as a pie-chart of the relative concentrations of the four possible [location,genotype] combinations; (B) shows nodes colored by their mean phenotypic value; (C) shows nodes colored by their mean DAP value; and (D) shows nodes colored by their mean temperature value. The mean values are also indicated within the respective circles. The size of the circle for each node is proportional to the size of the corresponding partial cluster. Also shown highlighted as thick colored edges are the set of interesting paths identified by our method. Edge directions are from low to high mean phenotypic values. The interesting paths are labeled as  $P_i\{s_1s_2\}$ , where  $i$  is the path number, and  $s_1s_2$  denotes the signature for that path ( $s_1$  corresponds to DAP and  $s_2$  corresponds to temperature). Recall that in the signature, 0 means decreasing and 1 means increasing.

Each segment of a pie chart reflects a specific individual and the area of a segment in that pie chart indicates the cardinality for that individual.

### C.2.2 Path analysis

On the topological object constructed using DAP and temperature as the double filter function, we identified multiple interesting paths using the method described in Section 3. Fig. A8 shows these paths that were automatically detected by different color-coded paths. Note that the signature along a path is fixed in this analysis (although our method has a feature to relax this condition). In what follows, we evaluate the qualitative significance of the interesting paths identified by our method, shown in Fig. A8:

- ❖ The collection of paths  $P_7, P_8$  essentially helps us to separate the points from the two locations. More specifically, the path  $P_7$  starts with points from both locations because their performances are very similar; however, after roughly 28 DAP (Fig. A8C), the points from KS separate and follow a different path compared to the points from NE.
- ❖ The sequence of paths  $[P_4, P_1]$ , which also includes the most interesting path by interestingness score ( $P_1$ ), represents the active growth period for the KS population is (Fig. A8B). In this period, the growth rate increased from 2.04 cm./DAP to 8.30 cm./DAP, from approximately 41 DAP to 61 DAP (see Fig. A8C). In contrast, the plants in NE, despite being the same genotype, had very low growth rates during roughly the same period in time (39 DAP to 62.5 DAP; see Figs. A8B, A8C).

For same time window the temperature in NE is almost similar to the temperature of KS (Fig. A8C, Fig. A8D)). Hence, temperature is not responsible for the variation of the plant growth rate in both locations.

- ❖ The sequence of paths  $[P_5, P_2, P_3]$  represents the active growth period of the NE population, where the growth rate increases from 1.23 cm./DAP to 6.87 cm./DAP (Fig. A8B). This high activity period starts from approx. 57 DAP and ends roughly at 81 DAP.
- ❖ Along the sequence of path  $[p_3, p_6]$ , the time (DAP) is gradually increasing (see Fig. A8C) but the phenotypic value (growth rate) increased swiftly along the path  $P_3$  (4.33 cm./DAP to 6.87 cm./DAP) and decreased slowly along the path  $P_6$  (6.87 cm./DAP to 6.36 cm./DAP), as can be seen in Fig. A8B. It coincides with the decrease in temperature from 96.66°F to 80.5°F and followed by increase from 80.5°F to 93°F (see Fig. A8D). Therefore, the optimal temperature for growth is 80.5°F.

To better illustrate this advantage, we overlaid the interesting path sequences identified by our paths (discussed above) on to the scatter plot. These path sequences are shown as arcs in Fig. A9. As can be seen, our interesting paths show three major “features” within this scatter plot:

- i) the period of active growth for [KS,B] between roughly 41 and 61 DAP
- ii) the period of active growth for [NE,B] appearing much later, between roughly 57 and 81 DAP; and
- iii) two subpopulations of [NE,B] meet at 80.5 DAP.

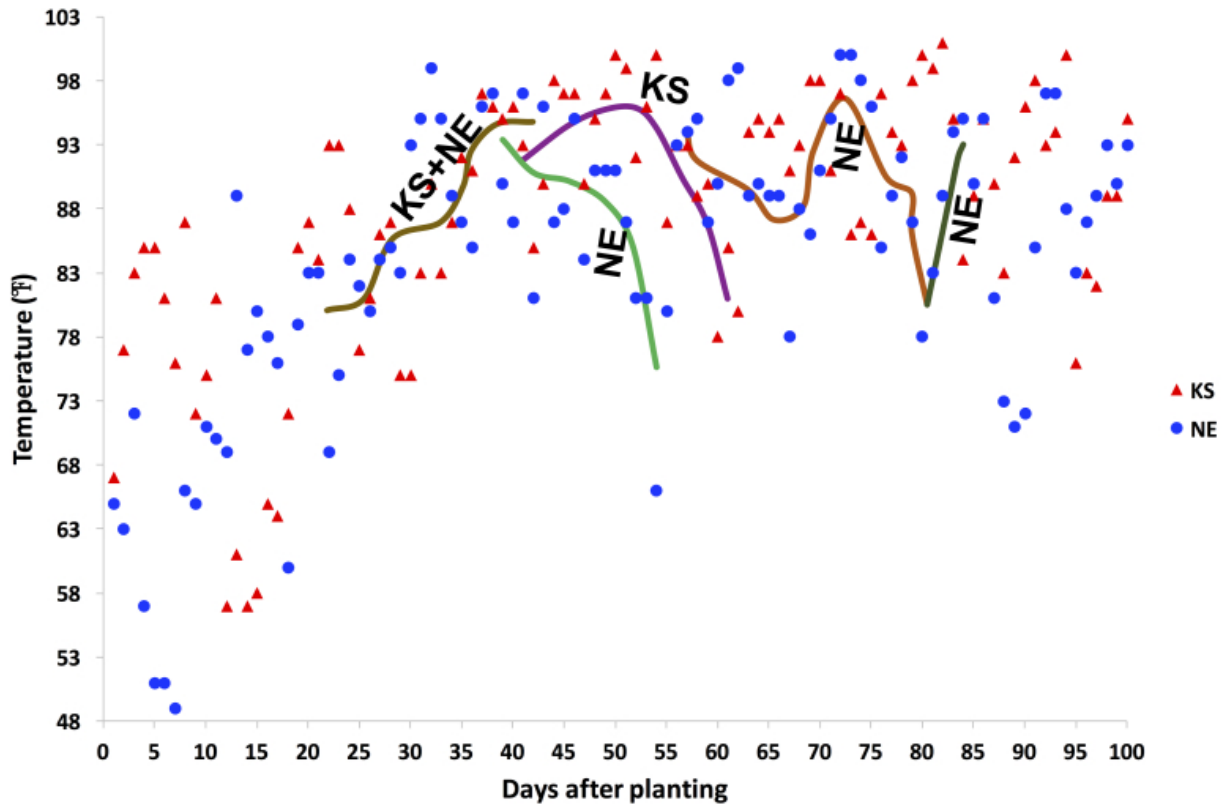


Figure A9: Scatter plot of data points with respect to DAP and temperature in both locations. The color of a point indicates the corresponding location. The paths generated from our TDA framework are placed here to reveal the phenotypic behavior.